

## Production of ethane and water in comet C/1996 B2 Hyakutake

Neil Dello Russo,<sup>1,2</sup> Michael J. Mumma,<sup>2</sup> Michael A. DiSanti,<sup>1,2</sup>  
and Karen Magee-Sauer<sup>3</sup>

Received 21 December 2001; revised 5 April 2002; accepted 29 May 2002; published 5 November 2002.

[1] Ethane (C<sub>2</sub>H<sub>6</sub>) and water (H<sub>2</sub>O) were detected in Comet C/1996 B2 Hyakutake between UT 1996 March 23.4 ( $R_h = 1.08$  AU preperihelion) and 1996 April 12.2 ( $R_h = 0.64$  AU preperihelion). Our long-slit infrared spectra featured both high spectral dispersion and high spatial resolution about the nucleus, permitting the extraction of rotational temperatures, production rates, and spatial distributions of species along the slit. Production rates were measured for water (on four dates) and ethane (on three dates). Their average relative abundance was  $C_2H_6/H_2O = (6.2 \pm 0.7) \times 10^{-3}$ . The spatial distributions of C<sub>2</sub>H<sub>6</sub> and H<sub>2</sub>O molecules in the coma were consistent with both species being released directly from the nucleus on all dates, although asymmetries about the nucleus are seen for both gas and dust. **INDEX TERMS:** 6005 Planetology: Comets and Small Bodies: Atmospheres—composition and chemistry; 6008 Planetology: Comets and Small Bodies: Composition; 6020 Planetology: Comets and Small Bodies: Ice; 6060 Planetology: Comets and Small Bodies: Radiation and spectra; **KEYWORDS:** Comets, infrared, spectroscopy, water, ethane, Hyakutake

**Citation:** Dello Russo, N., M. J. Mumma, M. A. DiSanti, and K. Magee-Sauer, Production of ethane and water in comet C/1996 B2 Hyakutake, *J. Geophys. Res.*, 107(E11), 5095, doi:10.1029/2001JE001838, 2002.

### 1. Introduction

[2] The long-period and dynamically new comets are thought to have formed in the 5–40 AU region of the protoplanetary nebula. The giant planets later scattered them into the Oort cloud where their bulk compositions remained chemically unaltered, owing to their great distance from the Sun (beyond  $\sim 10,000$  AU). Thus, their present compositions may reflect physical and chemical conditions in their formative region, which likely varied greatly with distance from the young Sun. For this reason, determining volatile compositions of comets is of primary importance to the study of our Solar System.

[3] Here, we report a detailed study of ethane (C<sub>2</sub>H<sub>6</sub>) and water (H<sub>2</sub>O) release in comet Hyakutake. Their distributions about the nucleus were measured at high spatial resolution, revealing the connection between the distribution of these species in the coma and their presence as native ices in the nucleus. Data obtained from observations on five dates provided absolute production rates and relative abundances for H<sub>2</sub>O and C<sub>2</sub>H<sub>6</sub>. This work also revises and extends results presented earlier for ethane and water production on UT 1996 March 24.5 [Mumma *et al.*, 1996]. Improved data processing techniques and new insights were used in the present analysis, including determination of production rates from off-nucleus extracts [Dello Russo *et al.*, 1998],

and the use of a temperature-dependent fluorescence model for determining C<sub>2</sub>H<sub>6</sub> Q-branch  $g$ -factors [Dello Russo *et al.*, 2001]. Application of these techniques enabled the determination of rotational temperatures, production rates, and mixing ratios. Analysis of the spatial distributions of species in the coma provides new insights into temporal variability of this comet.

### 2. Background

[4] Water is the dominant volatile species in most comets, and so its production rate and other properties (ortho-para ratio, rotational temperature) are of central importance in cometary science. Its production rate is often inferred from measurements of its photo-dissociation products, but these products can also be released from other parent species and their interpretations are sometimes subject to model uncertainties. Cometary H<sub>2</sub>O was first detected directly in 1P/Halley. Individual ro-vibrational lines of the  $\nu_3$  band of water were detected in Halley (and later in C/1987 VII Wilson) by high-dispersion infrared spectroscopy from NASA's Kuiper Airborne Observatory, helping to establish that water is the dominant cometary volatile [Mumma *et al.*, 1986; Larson *et al.*, 1989]. Later, H<sub>2</sub>O was detected in low-dispersion spectra acquired by IKS on the Vega-1 spacecraft, along with CO<sub>2</sub> and H<sub>2</sub>CO [Combes *et al.*, 1986, 1988]. The detection of CO<sub>2</sub> and water in C/1995 O1 (Hale-Bopp) with ISO again demonstrated the benefits of space observatories but also illustrated the limitations imposed by restricted observing opportunities and Sun-avoidance constraints [Crovisier *et al.*, 1997].

[5] The potential to observe water from ground-based observatories was suggested when nonresonant fluorescence (the 011–010 hot-band) emissions were detected at

<sup>1</sup>Department of Physics, Catholic University of America, Washington, D. C., USA.

<sup>2</sup>Laboratory for Extraterrestrial Physics, NASA Goddard Space Flight Center, Greenbelt, Maryland, USA.

<sup>3</sup>Department of Chemistry and Physics, Rowan University, Glassboro, New Jersey, USA.

2.65  $\mu\text{m}$  in KAO spectra of comets Halley and Wilson [Weaver *et al.*, 1987; Larson *et al.*, 1989]. These hot-bands are pumped from the ground vibrational level by infrared sunlight and they fluoresce into highly excited intermediate states that are not strongly populated in Earth's atmosphere. Subsequently, Bockelée-Morvan and Crovisier [1989] showed that a significant amount of the 2.8  $\mu\text{m}$  emission feature seen in low-dispersion ground-based spectra could be due to water hot-band emission. They suggested that such emissions might provide a convenient means for detecting water from ground-based observatories.

[6] Ground-based searches initially emphasized the  $\nu_1 + \nu_2 + \nu_3 - \nu_1$  (111–100) vibrational band near 2  $\mu\text{m}$ , which was accessible to a newly commissioned (in 1992) high-dispersion cryogenic infrared spectrometer (CSHELL) at IRTF. This approach proved successful; water was securely detected in comet C/1991 T2 Shoemaker-Levy, 6P/d'Arrest, and C/1996 B2 Hyakutake [Mumma *et al.*, 1995a, 1995b, 1996]. Water production rates were obtained for all three comets, and a rotational temperature was obtained for H<sub>2</sub>O in comet Hyakutake [Mumma *et al.*, 1996]. Our survey of the (1–0) band of CO at  $\sim 4.7$   $\mu\text{m}$  in Hyakutake revealed new strong emissions, which were identified as nonresonance fluorescence from the  $\nu_1 - \nu_2$  (100–010) and  $\nu_3 - \nu_2$  (001–010) hot-bands of H<sub>2</sub>O. Emissions from these two hot-bands had been predicted independently following the KAO results [Bockelée-Morvan and Crovisier, 1989].

[7] Spectral lines of four hot-bands have now been detected in comets. Reliable water production rates were obtained for Hale-Bopp, 21P/Giacobini-Zinner, C/1999 H1 (Lee), C/1999 S4 (LINEAR), and C/1999 T1 (McNaught-Hartley) [Weaver *et al.*, 1999a; Dello Russo *et al.*, 2000; Mumma *et al.*, 2001a, 2001b, 2001c]. This approach is now used routinely for measuring water production in comets.

[8] Symmetric hydrocarbons can only be detected at infrared wavelengths, but until recently, in-depth infrared studies of the organic composition of comets were difficult. The IKS infrared instrument flown on board the Vega 1 spacecraft detected a spectral signature in the 3.2–3.6  $\mu\text{m}$  region attributed to C-H stretching vibrations in one or more organic compounds [Combes *et al.*, 1986, 1988]. Subsequently, the 3.2–3.6  $\mu\text{m}$  emission feature was observed from the ground in Halley and several other comets with moderate spectral resolution [ $\lambda/\Delta\lambda \sim 100$ –1200, Brooke *et al.*, 1991; DiSanti *et al.*, 1995; Bockelée-Morvan *et al.*, 1995, and references therein].

[9] This organic feature was initially thought to arise from emission by solid organic (CHON) particles [Encrenaz and Knacke, 1991, and references therein], but examination of the strength of this feature as a function of heliocentric distance instead suggested a volatile origin [Chyba *et al.*, 1989]. The case for a volatile origin was strengthened with the detection of methanol in comet C/1989 X1 Austin [Hoban *et al.*, 1991; Bockelée-Morvan *et al.*, 1991]. Subsequent modeling of its  $\nu_2$ ,  $\nu_3$ , and  $\nu_9$  bands showed that methanol could contribute some (but not all) of the integrated flux measured in the X-CH feature [Reuter, 1992]. Presumably, fluorescent emissions from gas phase organic species other than methanol were also present, but detecting, isolating, and quantifying them was problematic at the low spectral resolution then available.

[10] Observations of comet Hyakutake with CSHELL (equipped with an improved InSb array by 1996) allowed the 2–5  $\mu\text{m}$  spectral region to be studied in a comet with unprecedented spectral resolution. This provided unambiguous detection of spectrally and spatially resolved ro-vibrational emissions from many previously known or suspected cometary constituents [Mumma *et al.*, 1996; Brooke *et al.*, 1996]. These observations also yielded some surprises. Strong Q-branches of ethane (C<sub>2</sub>H<sub>6</sub>) were detected while targeting  $\nu_2$  lines of methanol [Mumma *et al.*, 1996]. These and subsequent observations in comet Hale-Bopp established C<sub>2</sub>H<sub>6</sub> as an important cometary constituent and likely a significant contributor to the 3.2–3.6  $\mu\text{m}$  emission feature observed in many previous comets [Weaver *et al.*, 1999a; Dello Russo *et al.*, 2001]. Subsequently, C<sub>2</sub>H<sub>6</sub> was detected in four more comets (Giacobini-Zinner, Lee, LINEAR S4, and McNaught-Hartley), further establishing its role as a key organic volatile in comets [Weaver *et al.*, 1999b; Mumma *et al.*, 2000, 2001a, 2001b, 2001c].

### 3. Observations and Data Analysis

[11] Ro-vibrational lines from four water hot-bands were detected on four dates and seven ethane Q-branches from the  $\nu_7$  band were detected on three dates between UT 1996 Mar. 23.4 and Apr. 12.2 (Table 1). We used CSHELL at the NASA Infrared Telescope Facility on Mauna Kea, Hawaii [Greene *et al.*, 1993]. CSHELL has a  $256 \times 256$  pixel InSb array detector with a pixel size of 0.2", and provides spatial coverage along the 30" long slit which we oriented east-west. A 1" wide slit was used for our comet observations leading to a spectral resolving power  $\lambda/\Delta\lambda \sim 2 \times 10^4$ . At each grating setting, cometary data were acquired using a sequence of four scans (ABBA, where A is the source and B is the sky), with an integration time of 2 min on source per scan sequence. Sky spectra were obtained by nodding the telescope 2 arcmin from the source, providing sky cancellation via pixel-by-pixel subtraction. Flat-fields and dark frames were obtained immediately following each scan sequence. For each grating setting, spectra of infrared standard stars were obtained through a 4" wide slit for absolute flux calibration of the comet spectra.

[12] The data were processed using algorithms specifically tailored to our comet observations. Application of these has been described elsewhere [Dello Russo *et al.*, 1998, 2000, 2001; Magee-Sauer *et al.*, 1999; DiSanti *et al.*, 2001]. Initial processing included flat-fielding, and removal of high dark current pixels and cosmic ray hits. Spectral frames were registered such that the spectral dimension fell along rows and the spatial dimension fell along columns (Figure 1a). Spectra can then be extracted over any desired spatial extent and position along the slit (Figure 1b). Atmospheric models were obtained using the Spectrum Synthesis Program (SSP) [Kunde and Maguire, 1974] which accesses the HITRAN-1992 Molecular Database [Rothman *et al.*, 1992]. SSP models were used to assign wavelength scales to the extracted spectra, and to establish absolute column burdens for each significant absorbing species in the terrestrial atmosphere. The fully resolved model was binned to the instrumental sampling interval, convolved to the resolution of the comet spectrum and normalized to the cometary continuum (Figure 1b).

**Table 1.** CSHELL H<sub>2</sub>O and C<sub>2</sub>H<sub>6</sub> Observations in Comet C/1996 B2 Hyakutake

UT Date 1996	R <sub>h</sub> , AU	Δ, AU	Δ <sub>dot</sub> , km s <sup>-1</sup>	PA <sup>a</sup>	β <sup>b</sup>	H <sub>2</sub> O Hot-Band Lines	ν <sub>cs</sub> (cm <sup>-1</sup> ) <sup>c</sup>	I <sub>t</sub> (s) <sup>d</sup>
Mar 23.42	1.08	0.119	-30.1	238	43	2 <sub>02</sub> -3 <sub>03</sub> <sup>e</sup>	5080	240
Mar 23.43	1.08	0.119	-30.0	238	43	2 <sub>11</sub> -3 <sub>12</sub> <sup>e</sup>	5086	240
Mar 23.43	1.08	0.119	-30.0	238	43	2 <sub>02</sub> -3 <sub>03</sub> <sup>e</sup>	5066	240
Mar 23.45	1.08	0.119	-29.8	238	43	2 <sub>12</sub> -3 <sub>13</sub> <sup>e</sup>	5148	240
Mar 24.47	1.06	0.105	-15.0	225	52	3 <sub>13</sub> -4 <sub>14</sub> <sup>e</sup>	5080	240
Mar 24.48	1.06	0.105	-14.7	225	52	1 <sub>11</sub> -1 <sub>10</sub> <sup>e</sup>	5086	240
Mar 24.49	1.06	0.105	-14.5	225	52	2 <sub>02</sub> -3 <sub>03</sub> <sup>e</sup>	2149	60
Apr 11.19	0.662	0.565	+56.4	43	109	2 <sub>12</sub> -3 <sub>13</sub> <sup>e</sup>	5194	240
Apr 12.21	0.637	0.598	+56.6	42	109	1 <sub>11</sub> -1 <sub>10</sub> <sup>f</sup>	5194	120
						2 <sub>21</sub> -1 <sub>10</sub> <sup>g</sup>		
						2 <sub>02</sub> -1 <sub>01</sub> <sup>e</sup>		
						2 <sub>11</sub> -3 <sub>12</sub> <sup>h</sup>		
						3 <sub>13</sub> -4 <sub>14</sub> <sup>h</sup>		
						2 <sub>02</sub> -1 <sub>01</sub> <sup>e</sup>		
						2 <sub>11</sub> -3 <sub>12</sub> <sup>h</sup>		
						3 <sub>13</sub> -4 <sub>14</sub> <sup>h</sup>		
UT Date 1996	R <sub>h</sub> , AU	Δ, AU	Δ <sub>dot</sub> , km s <sup>-1</sup>	PA <sup>a</sup>	β <sup>b</sup>	C <sub>2</sub> H <sub>6</sub> ν <sub>7</sub> Q-Branches	ν <sub>cs</sub> (cm <sup>-1</sup> ) <sup>c</sup>	I <sub>t</sub> (s) <sup>d</sup>
Mar 24.45	1.06	0.106	-15.3	226	51	R <sub>Q</sub> <sub>0</sub> , P <sub>Q</sub> <sub>1</sub>	2984	240
Apr 10.20	0.686	0.533	+56.2	43	110	R <sub>Q</sub> <sub>3</sub> , iR <sub>Q</sub> <sub>4</sub>	2998	240
Apr 12.16	0.638	0.596	+56.5	42	109	R <sub>Q</sub> <sub>0</sub> , R <sub>Q</sub> <sub>1</sub>	2988	120
Apr 12.17	0.638	0.596	+56.5	42	109	R <sub>Q</sub> <sub>3</sub> , iR <sub>Q</sub> <sub>4</sub>	2998	120
Apr 12.19	0.638	0.597	+56.5	42	109	P <sub>Q</sub> <sub>2</sub> , P <sub>Q</sub> <sub>3</sub>	2979	120
Apr 12.20	0.637	0.597	+56.5	42	109	R <sub>Q</sub> <sub>0</sub> , P <sub>Q</sub> <sub>1</sub>	2984	120

<sup>a</sup> Position angle of the extended radius vector (degrees).<sup>b</sup> Sun-Comet-Earth angle (degrees).<sup>c</sup> Central wave number of the grating setting.<sup>d</sup> On source integration time in seconds.<sup>e</sup> Ro-vibrational line from the ν<sub>1</sub> + ν<sub>2</sub> + ν<sub>3</sub> - ν<sub>1</sub> water hot-band.<sup>f</sup> Ro-vibrational line from the ν<sub>3</sub> - ν<sub>2</sub> water hot-band.<sup>g</sup> Ro-vibrational line from the ν<sub>1</sub> - ν<sub>2</sub> water hot-band.<sup>h</sup> Ro-vibrational line from the 2ν<sub>2</sub> + ν<sub>3</sub> - ν<sub>2</sub> water hot-band.<sup>i</sup> The RQ<sub>3</sub> Q-branch was not used for quantitative analysis (see text).

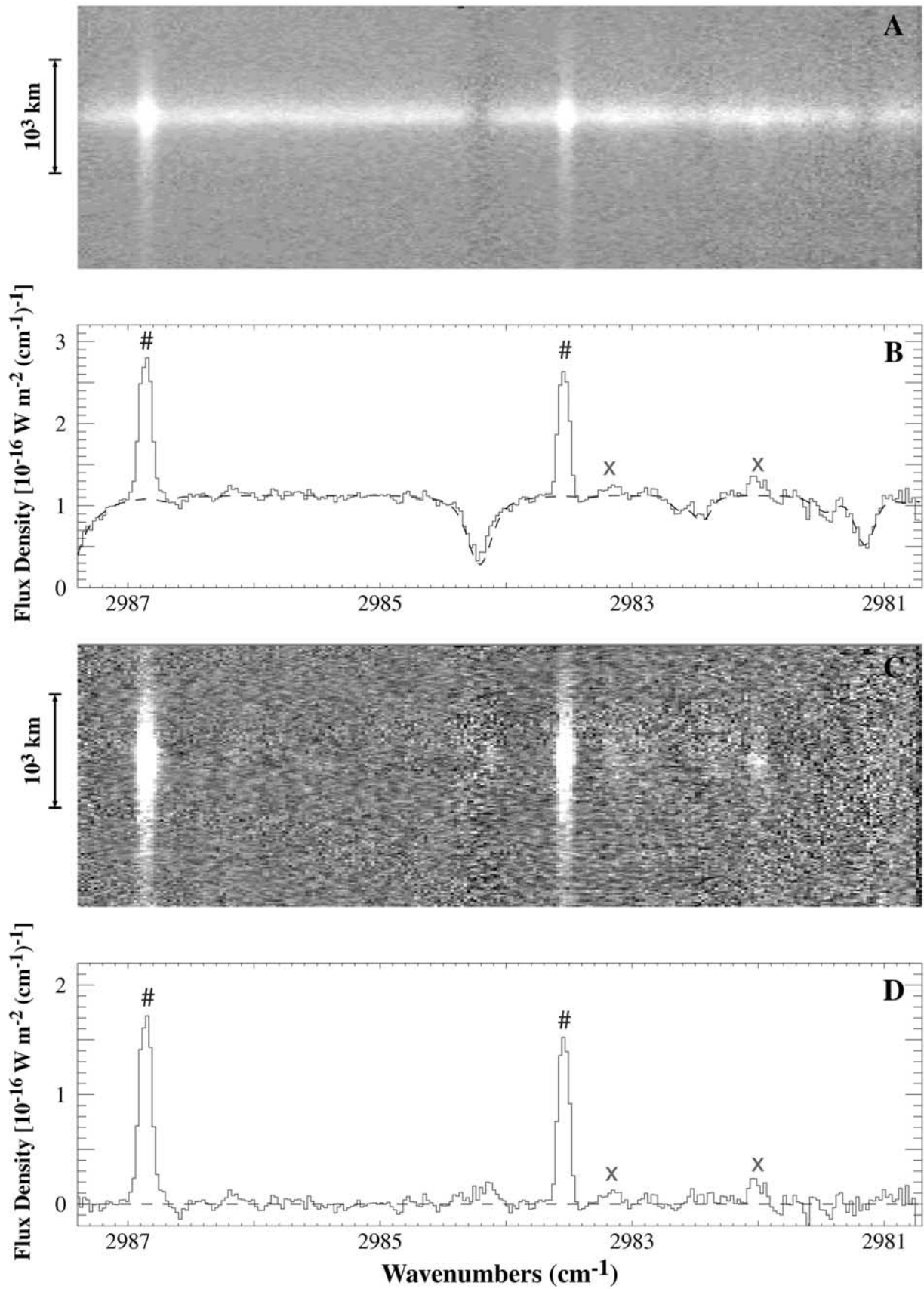
[13] Volatile emission features were separated from the continuum by subtracting the normalized atmospheric model from the comet spectrum row-by-row, yielding the net cometary molecular emissions still convolved with the atmospheric transmittance function (Figures 1c and 1d). The true line flux incident at the top of the terrestrial atmosphere was obtained from the observed flux by correcting for the monochromatic transmittance obtained from the fully resolved SSP model at the Doppler-shifted line position. The high resolution and sensitivity of CSHELL, coupled with the favorable apparition of comet Hyakutake, allowed detections of multiple water hot-band lines (Figure 2), and ethane Q-branches (Figure 3).

#### 4. Spatial Distribution of H<sub>2</sub>O and C<sub>2</sub>H<sub>6</sub> in Hyakutake

[14] Discerning different source contributions in the coma can reveal information on the physical nature and composition of the cometary nucleus. A more complete connection between nuclear ices and coma gases can be established by measuring the spatial distribution (or spatial profile) of a species in the coma. The close approach of comet Hyakutake to Earth in late March 1996 (Δ = 0.105 AU on UT March 24.5) allowed the distribution of species in the coma of Hyakutake to be sampled with high spatial resolution (each pixel represented ~15–18 km at the comet

on UT March 23 and 24). On UT April 10–12, as Hyakutake receded from Earth, spatial coverage at the comet was gained at the expense of spatial resolution (each pixel represented ~77–87 km at the comet on UT April 10–12).

[15] For spherically symmetric outflow at uniform velocity, the column density of a volatile (or dust) sublimated directly from the nucleus (with no additional distributed component) should fall off as ρ<sup>-1</sup>, where ρ is the projected distance from the nucleus. This is valid as long as ρ is small compared to the photodissociation scale length of the species (The scale length in km (λ<sub>s</sub>) = (τR<sub>h</sub><sup>2</sup>)(v<sub>gas</sub>R<sub>h</sub><sup>-0.6</sup>) where τ is the photodissociation lifetime (s), and v<sub>gas</sub> is the gas outflow velocity (km s<sup>-1</sup>) at R<sub>h</sub> = 1 AU). For ethane, τ ~ 9.1 × 10<sup>4</sup> s at R<sub>h</sub> = 1 AU [Huebner et al., 1992], and v<sub>gas</sub> ~ 0.8 km s<sup>-1</sup> at R<sub>h</sub> = 1 AU (cf. Biver et al. [1999] for gas outflow velocities and heliocentric dependences), therefore λ<sub>s</sub> ~ 4 × 10<sup>4</sup> km in Hyakutake on UT April 12. The spatial profile for a species with a significant distributed source will be broader, falling off more slowly than ρ<sup>-1</sup> (examples include OCS and CO in Hale-Bopp [Dello Russo et al., 1998; DiSanti et al., 1999, 2001], and CO in Hyakutake (M. A. DiSanti, M. J. Mumma, N. Dello Russo, K. Magee-Sauer, and D. Griep, Evidence for a dominant native source of carbon monoxide in comet Hyakutake, submitted to *Journal of Geophysical Research*, 2002). However, properties of the comet (e.g., jets), observing



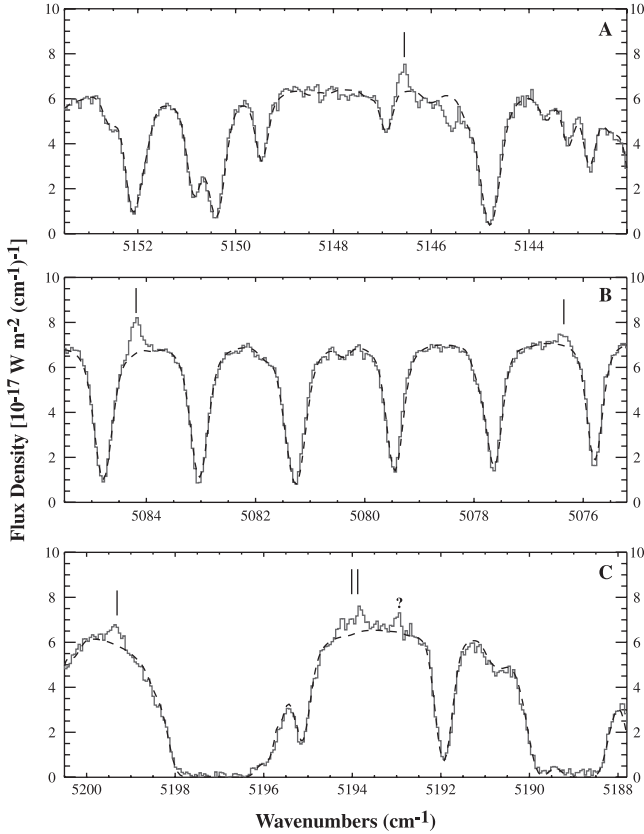


**Figure 2.** Detection of H<sub>2</sub>O hot-band lines in Hyakutake on three dates. Flux-calibrated cometary spectral extracts (solid curves). The displayed spectral extracts have a spatial extent of 1'' (five rows) and are centered on the nucleus. Cometary emission features are seen above the optimized atmospheric model spectra (dashed curves). Positions for expected H<sub>2</sub>O hot-band lines are marked and assignments are given below (from left to right). (a) UT 1996 March 23.45,  $\nu_1 + \nu_2 + \nu_3 - \nu_1$  ( $1_{11} - 1_{10}$ ). (b) UT 1996 March 24.47,  $\nu_1 + \nu_2 + \nu_3 - \nu_1$  ( $2_{02} - 3_{03}$ ),  $\nu_1 + \nu_2 + \nu_3 - \nu_1$  ( $2_{11} - 3_{12}$ ). (c) UT 1996 April 11.19,  $2\nu_2 + \nu_3 - \nu_2$  ( $2_{11} - 3_{12}$ ),  $2\nu_2 + \nu_3 - \nu_2$  ( $3_{13} - 4_{14}$ ),  $\nu_1 + \nu_2 + \nu_3 - \nu_1$  ( $2_{02} - 1_{01}$ ), and (?) unknown.

conditions, and optical depth effects [see *DiSanti et al.*, 2001] can also affect profile shapes, causing deviations from a  $\rho^{-1}$  distribution even for purely native species [*Dello Russo et al.*, 2000, 2001]. We have demonstrated that comparison of spatial profiles for volatile species and simultaneously measured (associated) dust can provide a

means for assessing the presence of a significant distributed source. However, such comparisons cannot reliably reveal the presence of small contributions by distributed sources close to the nucleus [see *DiSanti et al.*, 1999, 2001; *Dello Russo et al.*, 2000, 2001 for detailed discussion].

[16] Following their release from the nucleus, collisions tend to isotropize the outflowing gas more rapidly than the dust [*Xie and Mumma*, 1996]. So, in general, asymmetries in spatial profiles are more severe for dust than for parent volatiles. Figure 4 shows spatial profiles for H<sub>2</sub>O on UT March 23.4 and 24.5, and C<sub>2</sub>H<sub>6</sub> on UT March 24.5 and April 12.2 (spatial profiles were also obtained on other dates as listed in Table 1, but the profiles in Figure 4 represent the highest signal-to-noise measurements). Spatial profiles of the associated dust continuum were also obtained for comparison.

[17] On UT March 23.4, the spatial profiles of water and the associated dust closely follow a  $\rho^{-1}$  distribution beyond  $\sim 1''$  from the nucleus (the region within  $\sim 1-2''$  is affected by seeing), indicating that most (if not all) water seen in the coma was released directly from the nucleus (Figure 4a). The lack of significant asymmetries in these spatial profiles also suggests that the comet was in a relatively quiescent state during these observations.

[18] In contrast to the previous date, observations on UT March 24.5 show evidence for asymmetric outflow in both the gas and dust. The C<sub>2</sub>H<sub>6</sub> spatial profile (observed on UT 10:49 March 24) shows a significant enhancement to the west of the nucleus, while the associated dust shows a small enhancement to the east (Figure 4c). Observations obtained  $\sim 30$  min later reveal a slight H<sub>2</sub>O enhancement to the west (between  $\sim 100$  and 400 km from the nucleus), and no obvious dust enhancement (Figure 4b). Observations targeting CH<sub>4</sub> and CH<sub>3</sub>OH taken 10 and 40 min, respectively, before the ethane observation reveal even larger volatile enhancements to the west (Figure 4c). Since CH<sub>4</sub> and CH<sub>3</sub>OH are not expected to have significant distributed source contributions in the coma (and they show no evidence for a distributed source in subsequently observed comets), the enhancements in the C<sub>2</sub>H<sub>6</sub>, CH<sub>4</sub>, and CH<sub>3</sub>OH spatial profiles are likely due to jet activity and not to the presence of distributed sources. This is also supported by the fact that the C<sub>2</sub>H<sub>6</sub> spatial profile on UT April 12.2 follows a  $\rho^{-1}$  distribution and that no distributed source for C<sub>2</sub>H<sub>6</sub> has been seen in other comets (we note, however, that we cannot rule out distributed sources with short scale lengths). The smaller enhancement seen in the H<sub>2</sub>O spatial profile compared with C<sub>2</sub>H<sub>6</sub> (observed  $\sim 30$  min earlier) suggests that the comet may have been in a more quiescent state (along the east-west direction) at the time of the water

**Figure 1.** (opposite) Detection of C<sub>2</sub>H<sub>6</sub> in Comet Hyakutake on UT 1996 March 24.45. (a) On-chip spatial-spectral image showing molecular emissions and the dust continuum. The spatial dimension is along columns and the spectral dimension is along rows. The spatial extent of the image is  $\sim 30''$  on the sky, with a spatial scale displayed on the left. East is at the top. (b) Flux-calibrated cometary spectral extract (solid curve). The displayed spectral extract has a spatial extent of 1'' (five rows) and is centered on the nucleus. Cometary emissions are clearly seen above the optimized atmospheric model spectrum (dashed curve). The identified lines from left to right are (#) C<sub>2</sub>H<sub>6</sub>  $\nu_7^R Q_0$ , (#) C<sub>2</sub>H<sub>6</sub>  $\nu_7^P Q_1$ , (x) CH<sub>3</sub>OH  $\nu_9$  ( $K = -2 \leftarrow -1$  E), (x) CH<sub>3</sub>OH  $\nu_2$  ( $K = 2 \leftarrow 3$  A). (c) The residual spectral image shown in Figure 1a after removal of the dust continuum via row-by-row scaled subtraction of the atmospheric model. (d) Flux-calibrated residual spectral extract. The displayed residual spectrum has a spatial extent of 1'' (five rows) and is centered on the nucleus. C<sub>2</sub>H<sub>6</sub> (#) and CH<sub>3</sub>OH (x) cometary emission lines are noted.

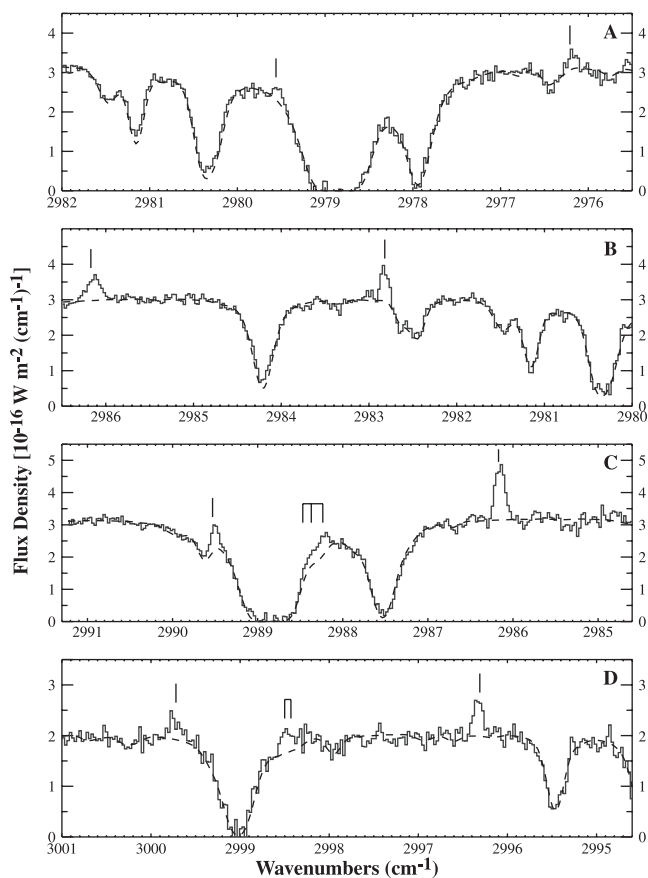


**Figure 3.** Flux-calibrated spectra of comet Hyakutake representing four grating settings which together show the detection of seven  $C_2H_6$   $\nu_7$  Q-branches and lines of  $CH_4$   $\nu_3$  on UT 1996 April 12.2. The displayed spectral extracts have a spatial extent of  $1''$  (five rows) and are centered on the nucleus. Each panel shows cometary continuum and molecular emission (solid curves), and a normalized atmospheric transmittance spectrum (dashed curves). Positions for expected cometary emissions are marked and assignments are given below (from left to right). (a)  $C_2H_6$   $\nu_7^P Q_2$ ,  $C_2H_6$   $\nu_7^P Q_3$ . (b)  $C_2H_6$   $\nu_7^R Q_0$ ,  $C_2H_6$   $\nu_7^P Q_1$ . (c)  $C_2H_6$   $\nu_7^R Q_1$ ,  $CH_4$   $\nu_3$  P3 (F<sub>1</sub>, F<sub>2</sub>, A<sub>2</sub>),  $C_2H_6$   $\nu_7^R Q_0$ . (d)  $C_2H_6$   $\nu_7^R Q_4$ ,  $CH_4$   $\nu_3$  P2 (E, F<sub>2</sub>),  $C_2H_6$   $\nu_7^R Q_3$  [blended with OH (1-0, J = P12.5 2<sup>-</sup>) and  $CH_3OH$   $\nu_2$  (K = 0 ← 1 A)].

measurements. The nuclear rotation period of 6.23 hours [Schleicher *et al.*, 1998] implies rotation by  $\sim 30^\circ$  in 30 min. An individual vent could experience a major change in insolation during that time interval, with consequent changes in production.

[19] On UT April 12.2, the spatial coverage is larger by about a factor of six ( $1'' = 433$  km) due to the larger geocentric distance of the comet. The spatial profile of  $C_2H_6$  on this date closely follows a  $\rho^{-1}$  distribution beyond the seeing-affected region, while the associated dust shows a significant enhancement in the west direction (Figure 4d). We note that dust enhancements on UT March 24.5 and April 12.2 were in the sunward direction, while the gas enhancements from March 24.5 were antisunward (Figure 4). An analysis and comparison of  $H_2O$ ,  $C_2H_6$ , and dust spatial profiles on these dates suggest a primarily native

source for both water and ethane in comet Hyakutake with some significant outflow asymmetries present most notably on UT March 24.5 (Figure 4).

## 5. Production Rates

[20] We determine “global” production rates from the measured line intensities in the following way. The high spatial resolution afforded by CSHELL allows “spherical” production rates for strong emissions to be determined at different positions along the slit. For this purpose, we assume that  $H_2O$  and  $C_2H_6$  are produced at the nucleus and flow outward with spherical symmetry and with uniform velocity. A spherical production rate is determined from the flux contained within a  $1'' \times 1''$  box. When this box is stepped at  $1''$  intervals along the slit, the sequence of spherical production rates constitutes a Q-curve [Figures 5a

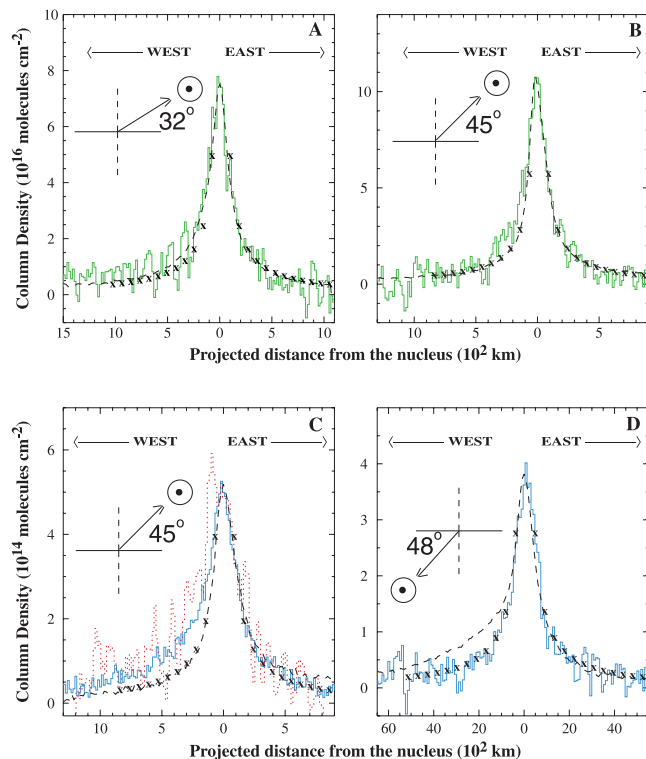


**Figure 4.** Spatial profiles for  $H_2O$  (solid green curves) and  $C_2H_6$  (solid blue curves) and associated dust (dashed black curves) in comet Hyakutake. (a) Spatial profiles for  $H_2O$  and dust on UT 1996 March 23.4. (b) Spatial profiles for  $H_2O$  and dust on UT 1996 March 24.5. (c) Spatial profiles for  $C_2H_6$  and dust on UT 1996 March 24.5. A spatial profile for  $CH_3OH$  from a grating setting taken 40 min prior to the  $C_2H_6$  observation is also shown (dotted red curve). (d) Spatial profiles for  $C_2H_6$  and dust on UT 1996 April 12.2. A  $\rho^{-1}$  distribution (x) is also shown at intervals of  $1''$  on all plots. The  $C_2H_6$  profiles incorporate all Q-branches measured on a particular date. The  $H_2O$  profiles incorporate all lines except the lines at  $5 \mu m$  on UT March 24.49. The slit was oriented east-west on all dates. The direction of the Sun with respect to the comet is indicated with a compass on the left side of each figure.

**Table 2.** Derived Line Fluxes and Production Rates From Water Hot-Band Lines and  $\nu_7$  Ethane Q-Branched in Comet Hyakutake

UT Date 1996	Infrared Flux Standard Stars <sup>a</sup>	H <sub>2</sub> O Hot-Band Lines	g-Factor, 10 <sup>-8</sup> s <sup>-1</sup>	Line Flux, 10 <sup>-18</sup> W m <sup>-2</sup> <sup>b</sup>	Q, 10 <sup>29</sup> mol s <sup>-1</sup> <sup>c</sup>
Mar. 23.42	BS 4550 (CF Uma)	2 <sub>02</sub> -3 <sub>03</sub> <sup>d</sup>	1.54	5.90 ± 0.21	1.89 ± 0.21
Mar. 23.42		2 <sub>11</sub> -3 <sub>12</sub> <sup>d</sup>	0.56	2.92 ± 0.34	2.55 ± 0.52
Mar. 23.43	BS 4550	2 <sub>02</sub> -3 <sub>03</sub> <sup>d</sup>	1.54	6.05 ± 0.31	1.93 ± 0.29
Mar. 23.43		2 <sub>12</sub> -3 <sub>13</sub> <sup>d</sup>	0.36	1.48 ± 0.23	1.99 ± 0.67
Mar. 23.43		3 <sub>13</sub> -4 <sub>14</sub> <sup>d</sup>	0.75	2.73 ± 0.20	1.80 ± 0.36
Mar. 23.45		1 <sub>11</sub> -1 <sub>10</sub> <sup>d</sup>	0.86	3.91 ± 0.31	2.19 ± 0.43
Mar. 24.47		2 <sub>02</sub> -3 <sub>03</sub> <sup>d</sup>	1.53	8.07 ± 0.32	2.24 ± 0.17
Mar. 24.47		2 <sub>11</sub> -3 <sub>12</sub> <sup>d</sup>	0.56	3.81 ± 0.34	2.88 ± 0.52
Mar. 24.48		2 <sub>02</sub> -3 <sub>03</sub> <sup>d</sup>	1.53	9.51 ± 0.22	2.63 ± 0.18
Mar. 24.48		2 <sub>12</sub> -3 <sub>13</sub> <sup>d</sup>	0.36	2.42 ± 0.20	2.82 ± 0.44
Mar. 24.49		1 <sub>11</sub> -1 <sub>10</sub> <sup>e</sup>	49.1	96.4 ± 6.6	2.75 ± 0.30
Mar. 24.49		2 <sub>21</sub> -1 <sub>10</sub> <sup>f</sup>	14.1	28.3 ± 6.5	1.80 ± 0.54
Apr. 11.19	BS 2560(15 Lyn)	g <sup>g</sup>	6.73	22.2 ± 1.0	4.17 ± 0.42
Apr. 12.21	BS 2560	g	6.70	20.7 ± 1.9	3.99 ± 0.76

UT Date 1996	Infrared Flux Standard Stars <sup>a</sup>	$\nu_7$ Q-Branch Assignment	g-Factor, 10 <sup>-5</sup> s <sup>-1</sup>	Line Flux, 10 <sup>-17</sup> W m <sup>-2</sup> <sup>b</sup>	Q, 10 <sup>28</sup> mol s <sup>-1</sup> <sup>c</sup>
Mar. 24.45	BS 4550	<sup>R</sup> Q <sub>0</sub>	3.36	9.16 ± 1.06	1.97 ± 0.33
		<sup>P</sup> Q <sub>1</sub>	3.01	6.95 ± 0.81	1.67 ± 0.29
Apr. 10.20	BS 2560	<sup>R</sup> Q <sub>4</sub>	1.07	1.13 ± 0.15	2.21 ± 0.37
Apr. 12.20	BS 2560	<sup>R</sup> Q <sub>0</sub>	3.30	3.39 ± 0.38	2.24 ± 0.30
Apr. 12.16		<sup>R</sup> Q <sub>0</sub>	3.30	3.89 ± 0.45	2.55 ± 0.36
Apr. 12.16		<sup>R</sup> Q <sub>1</sub>	2.80	3.68 ± 0.53	2.86 ± 0.47
Apr. 12.17		<sup>R</sup> Q <sub>4</sub>	1.08	1.27 ± 0.22	2.55 ± 0.49
Apr. 12.20		<sup>P</sup> Q <sub>1</sub>	2.96	2.98 ± 0.36	2.20 ± 0.32
Apr. 12.19		<sup>P</sup> Q <sub>2</sub>	2.78	3.04 ± 0.43	2.40 ± 0.39
Apr. 12.19		<sup>P</sup> Q <sub>3</sub>	2.10	2.08 ± 0.29	2.17 ± 0.36

<sup>a</sup> BS numbers are given with the star name in parentheses. The same calibration stars were used for each grating setting on a particular date.

<sup>b</sup> Total transmittance corrected flux 1.5''–11.5'' off the nucleus in both the east and west directions. This includes ten 1'' × 1'' boxes (the first box is centered at 2'' off the nucleus) stepped outward in each direction (the final box is centered at 11'' off the nucleus). The total aperture size is therefore 20'' × 1''.

<sup>c</sup> Production rates derived by stepping 1'' × 1'' extracts between 1.5''–11.5'' off the nucleus at 1'' intervals in both the east and west directions for each measured line. These values are the weighted average of production rates obtained within each of these twenty 1'' × 1'' boxes.

<sup>d</sup> Ro-vibrational lines from the  $\nu_1 + \nu_2 + \nu_3 - \nu_1$  water hot-band.

<sup>e</sup> Ro-vibrational line from the  $\nu_3 - \nu_2$  water hot-band.

<sup>f</sup> Ro-vibrational line from the  $\nu_1 - \nu_2$  water hot-band.

<sup>g</sup> g-factors, line fluxes, and production rates given for the three lines listed for these dates in Table 1.

and 6a; also see *Dello Russo et al.*, 1998, 2000, 2001; *Magee-Sauer et al.*, 1999; *DiSanti et al.*, 2001].

[21] The production rate (molecules s<sup>-1</sup>) at a given step is calculated as follows

$$Q = \frac{4\pi\Delta^2 F_i}{g_i \tau (h\nu) f(x)} \quad (1)$$

[22] The geocentric distance  $\Delta$  is in meters,  $h\nu$  is the energy (J) of a photon with wave number  $\nu$  (cm<sup>-1</sup>), and  $f(x)$  is the fraction of molecules expected in the sampled region ( $x$  being the fraction of a photodissociation scale length subtended by the aperture radius; see appendix of *Hoban et al.*, 1991). The photodissociation lifetime  $\tau$  (s) and line g-factor  $g_i$  (photons s<sup>-1</sup> molecule<sup>-1</sup>) are both calculated for  $R_h = 1$  AU. While the band-integrated g-factor is nearly independent of temperature, the evaluation of g-factors for individual lines requires knowledge of the rotational temperature and a quantum-band model. The flux (W m<sup>-2</sup>) from the  $i$ th line incident atop the terrestrial atmosphere is denoted  $F_i$ . A small correction factor (15%) is applied to account for flux that falls outside the five columns extracted for a given molecular emission line (the image of a spectral line is slightly broader than the 1'' slit width). Transmittance-corrected fluxes are given in Table 2 for each meas-

ured ethane Q-branch and water hot-band line. When sufficient lines were sampled on a particular date, a rotational temperature was derived, on other dates a reasonable rotational temperature was adopted (Table 3).

[23] Q-curves for C<sub>2</sub>H<sub>6</sub> and H<sub>2</sub>O were derived using g-factors obtained from fluorescence models for these molecules at the appropriate rotational temperature [*Mumma et al.*, 1995a; *Dello Russo et al.*, 2000, 2001; Table 2]. For an aperture diameter much smaller than the destruction scale length,  $f(x) \propto (\tau v_{\text{gas}})^{-1}$ ; inspection of equation (1) shows that our derived Q values are not sensitive to the lifetime assumed but they are sensitive to the outflow velocity. We adopted a gas outflow velocity consistent with measurements at radio wavelengths for Hyakutake [ $v_{\text{gas}} = 0.8 R_h^{-0.6}$  km s<sup>-1</sup>; *Biver et al.*, 1999], and we adopted the standard photodissociation lifetime for quiet Sun conditions [ $\tau_{\text{C}_{2\text{H}_6}} = 9.1 \times 10^4$  s,  $\tau_{\text{H}_2\text{O}} = 8.3 \times 10^4$  s at  $R_h = 1$  AU; *Huebner et al.*, 1992]. Dust Q-curves were generated using the simultaneously obtained continuum profile and assuming  $\tau_{\text{dust}} \gg \tau_{\text{gas}}$  (Figures 5a and 6a).

[24] ‘‘Symmetric’’ production rates were determined for H<sub>2</sub>O (Figure 5b) and C<sub>2</sub>H<sub>6</sub> (Figure 6b) by taking a weighted mean of spherical production rates at corresponding distances from the nucleus in the east and west directions ( $Q_{\text{dust}}$  is scaled to  $Q_{\text{gas}}$  at the nucleus centered position in

**Table 3.** Rotational Temperatures, Production Rates, and Relative Abundances for Ethane and Water in Comet Hyakutake

UT Date 1996	$T_{\text{rots}}$ K	$10^{27} \frac{Q(\text{C}_2\text{H}_6)}{\text{mol s}^{-1}}$	$10^{27} \frac{Q(\text{H}_2\text{O})}{\text{mol s}^{-1}}$	$\text{C}_2\text{H}_6/\text{H}_2\text{O}, 10^{-3}$
Mar. 23.42–23.45	$89 \pm 21^{\text{a}}$		$200 \pm 23^{\text{a}}$ $312^{\text{b}}$ $180^{\text{c}}$	
Mar 24.45–25.49	$90^{\text{d,e}}$	$1.82 \pm 0.31^{\text{a,c}}$	$254 \pm 25^{\text{a,c}}$ $249–334^{\text{f}}$ $277^{\text{b}}$	$7.2 \pm 1.4^{\text{a,c}}$
Apr 10.20	$90^{\text{d}}$	$2.21 \pm 0.37^{\text{a}}$	$173–257^{\text{f}}$ $280^{\text{c}}$	
Apr 11.19	$90^{\text{d}}$		$417 \pm 42^{\text{a}}$ $474^{\text{d}}$	$5.6 \pm 1.0^{\text{a,g}}$
Apr 12.16–12.21	$93 \pm 19^{\text{a}}$	$2.37 \pm 0.19^{\text{a}}$	$399 \pm 76^{\text{a}}$ $493^{\text{b}}$ $310^{\text{c}}$	$5.9 \pm 1.3^{\text{a}}$

<sup>a</sup> Measurements based on this work. Global production rates for a particular date are calculated from the weighted average of values obtained from individual line measurements on that date (as listed in Table 2). Rotational temperatures are derived for water on UT Mar. 23.4, and for ethane on UT Apr. 12.2.

<sup>b</sup> Based on O(<sup>1</sup>D) measurements on UT 1996 Mar. 23.44, Mar. 24.40, Apr. 11.14, and Apr. 12.14 [Hicks and Fink, 1997].

<sup>c</sup> Based on H Ly  $\alpha$  measurements on UT 1996 Mar. 23, Apr. 10, and Apr. 12 [Bertaux et al., 1998].

<sup>d</sup> Adopted rotational temperatures.

<sup>e</sup> We derived rotational temperatures for HCN ( $83 \pm 9$  K for a nucleus-centered extract) and CO ( $59 \pm 3$  K for an extract  $5''–11''$  off the nucleus) on UT March 24.5 [Magee-Sauer et al., 2002; DiSanti et al., 2002]. If the rotational temperature is as low as 60 K for C<sub>2</sub>H<sub>6</sub> and H<sub>2</sub>O on UT March 24.5:  $Q(\text{C}_2\text{H}_6) = 1.52 \pm 0.26$ ,  $Q(\text{H}_2\text{O}) = 207 \pm 21$ ,  $\text{C}_2\text{H}_6/\text{H}_2\text{O} = 7.3 \pm 1.4$  (in units as given in the column head of the table).

<sup>f</sup> OH production rates on UT 1996 Mar. 24.10 and Apr. 9.57 [Gérard et al., 1998]. The ranges in production rates reflect calculations with different Haser parameters.

<sup>g</sup> Based on a weighted average of ethane production rates on UT 1996 Apr 10.20, and Apr 12.2.

Figures 5 and 6). Opacity effects were determined to be negligible for all lines except for the H<sub>2</sub>O  $\nu_3 - \nu_2$  ( $1_{11} - 1_{10}$ ) line observed on UT March 24.5. Optical depth effects for water hot-band emissions are caused by opacity in the pumping transitions and are negligible in the radiating transitions [Dello Russo et al., 2000]. The intensity of the  $\nu_3 - \nu_2$  ( $1_{11} - 1_{10}$ ) line was corrected for opacity, as discussed in DiSanti et al. [2001] (this correction increased the production rate derived from this line by 40%).

[25] The  $Q$ -curves for dust, H<sub>2</sub>O, and C<sub>2</sub>H<sub>6</sub> (as well as those for other volatile species) show that production rates derived from nucleus-centered extracts are lower than those derived at positions offset from the nucleus, due to seeing, drift, and other factors associated with real observing conditions [see Dello Russo et al., 1998, 2000 for detailed discussion]. Typically, symmetric production rates reached a constant (terminal) value near  $2''$  from the nucleus, and nucleus-centered values are typically a factor of 2–5 lower than terminal values (Figures 5 and 6). For this reason, the “global” production rates determined from each individual  $Q$ -branch of C<sub>2</sub>H<sub>6</sub> and hot-band line of H<sub>2</sub>O were taken from a weighted average of symmetric production rates over the range  $1.5''–11.5''$  from the nucleus. This includes ten  $1'' \times 1''$  boxes on each side of the nucleus for a total effective aperture size of  $20'' \times 1''$  for fluxes and production rates reported in Table 2. Although asymmetries will likely have a small effect on our derived global production rates, this method has been shown to be a valid approach to first order [cf. Xie and Mumma, 1996]. Global production rates for a particular date (Table 3) are represented by the weighted average of values obtained from individual line measurements on that date, as listed in Table 2. The <sup>R</sup>Q<sub>3</sub>  $Q$ -branch was not used in this analysis since it is blended with lines of CH<sub>3</sub>OH and OH whose intensities are unknown.

[26] In order to demonstrate the effects of seeing on measured production rates along the slit (and separate seeing effects from jet activity), we compare volatile and dust  $Q$ -curves with a  $Q$ -curve derived from a measured stellar profile convolved with a  $\rho^{-1}$  distribution ( $x$  in Figures 5 and 6). We note that it is probable that conditions were not identical for stellar and cometary observations (which were taken about 2 hours apart on UT March 24.5), however  $Q$ -curves obtained for volatiles and dust are similar to that derived from the convolved PSF (Figures 5 and 6). This demonstrates that seeing is primarily responsible for lower production rates derived from nucleus-centered extracts and for the general rise to a terminal value in the C<sub>2</sub>H<sub>6</sub>, H<sub>2</sub>O, and dust  $Q$ -curves. Despite general similarities, small differences in volatile and dust  $Q$ -curves from that of the convolved PSF are often seen (Figures 5 and 6). This suggests that effects other than seeing also influence gas and dust  $Q$ -curves. On UT March 24.5, relative to a convolved PSF  $Q$ -curve, C<sub>2</sub>H<sub>6</sub> and the associated dust  $Q$ -curves rise to higher terminal values than do  $Q$ -curves for H<sub>2</sub>O and its associated dust (Figures 5 and 6). This is likely the signature of variable activity in the comet suggesting it may have been more active (within the slit) during the C<sub>2</sub>H<sub>6</sub> observations (C<sub>2</sub>H<sub>6</sub> and H<sub>2</sub>O were sampled about 30 min apart on this date).

[27] Errors were evaluated on each date for all detected C<sub>2</sub>H<sub>6</sub> and H<sub>2</sub>O lines. The ( $1\sigma$ ) errors in  $Q$ -branch flux reported in Table 2 were derived from the deviation of the C<sub>2</sub>H<sub>6</sub> and H<sub>2</sub>O spatial profiles (Figure 4) from a fitted curve (gaussian + polynomial). The uncertainty in global production rate was determined by comparing the standard deviation of the mean production rate over the range  $1.5''–11.5''$  from the nucleus to the stochastic error due to photon noise and taking the higher value. In general, for these high (stochastic)

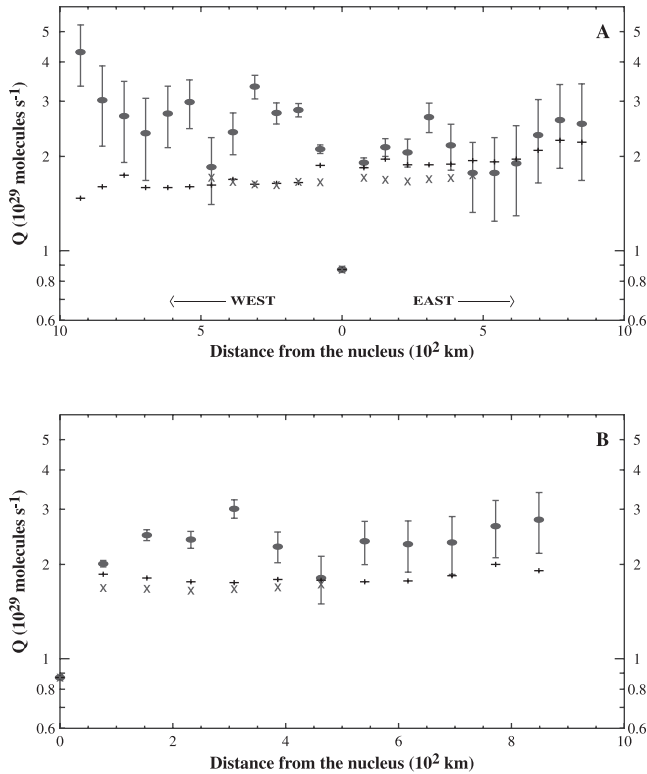


**Figure 5.** Q-curves for H<sub>2</sub>O (circles), associated dust (+), and a representative stellar spatial profile (PSF) convolved with a  $\rho^{-1}$  distribution (x) in comet Hyakutake on UT 1996 March 24.5. (a) H<sub>2</sub>O, dust, and convolved PSF spherical Q-curves. (b) H<sub>2</sub>O, dust, and convolved PSF symmetric Q-curves. Spherical production rates are derived by stepping  $1'' \times 1''$  extracts east and west of the nucleus out to  $\sim 11''$ . Symmetric production rates are derived from a weighted average of east and west extracts. The nucleus-centered dust and convolved PSF “production rates” are scaled to the nucleus centered production rate of H<sub>2</sub>O. The convolved PSF simulates the effects of seeing on Q-curves.

signal-to-noise data, the error was dominated by the standard deviation of the mean production rate over the range  $1.5''$ – $11.5''$  from the nucleus. This includes factors such as deviations in the synthetic atmospheric model fit, instrumental effects, spatial variations in rotational temperature and outflow velocity, and other factors that cause deviations from our idealized gas outflow model. On dates where insufficient lines were detected to determine a rotational temperature, a minimum uncertainty of 10% in the production rate was assumed (For ethane and water lines most sensitive to an assumed rotational temperature of 90 K, a change in assumed  $T_{\text{rot}}$  of  $\sim \pm 12$  K will change the derived production rate by 10%).

## 6. Discussion

[28] Ethane production rates were derived on three dates (Table 3), culminating with the detection of seven  $\nu_7$  Q-branches on UT 1996 April 12.2 (Figure 3). The average relative abundance of  $C_2H_6/H_2O = (6.2 \pm 0.7) \times 10^{-3}$ . Production of  $C_2H_6$  by gas-phase ion-molecule reactions is

energetically forbidden at the low temperatures characteristic of dense interstellar cloud cores, so the discovery of abundant  $C_2H_6$  in comet Hyakutake implies its ices did not originate in this way [Mumma *et al.*, 1996]. In addition, the abundances of related hydrocarbons (e.g., CH<sub>4</sub>, C<sub>2</sub>H<sub>2</sub>, CO, and CH<sub>3</sub>OH) argued against formation in a thermochemically equilibrated region of the solar nebula. Therefore, it is likely that  $C_2H_6$  formed on icy grain mantles in the natal cloud (or the distant solar nebula) by photolysis of CH<sub>4</sub> or by H-atom addition reactions to C<sub>2</sub>H<sub>2</sub> [Mumma *et al.*, 1996].

[29] Since its initial discovery in comet Hyakutake,  $C_2H_6$  has been seen in seven long-period comets (e.g., Hale-Bopp, Lee, LINEAR S4, and McNaught Hartley) and short-period comet Giacobini-Zinner [Mumma *et al.*, 2000, 2001a, 2001b, 2001c; Dello Russo *et al.*, 2001]. The abundance of ethane in comets and the strength of its  $\nu_7$  and  $\nu_5$  bands has important implications for the interpretation of the 3.2–3.6  $\mu\text{m}$  X-CH feature seen in many comets with low and moderate spectral resolutions [cf. Reuter, 1992; DiSanti *et al.*, 1995; Bockelée-Morvan *et al.*, 1995; Weaver *et al.*, 1999c; Dello Russo *et al.*, 2001].  $C_2H_6$  can account for much of the unexplained excess

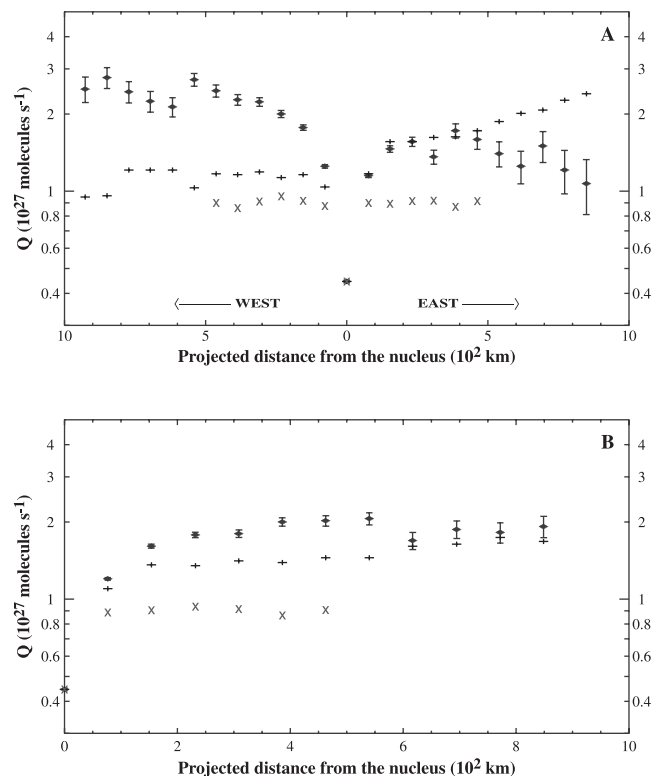


**Figure 6.** Q-curves for  $C_2H_6$  (diamonds), associated dust (+), and a representative stellar spatial profile (PSF) convolved with a  $\rho^{-1}$  distribution (x) in comet Hyakutake on UT 1996 March 24.5. (a)  $C_2H_6$ , dust, and convolved PSF spherical Q-curves. (b)  $C_2H_6$ , dust, and convolved PSF symmetric Q-curves. The nucleus-centered dust and convolved PSF “production rates” are scaled to the nucleus centered production rate of  $C_2H_6$ . The convolved PSF Q-curve reaches a significantly lower terminal value than  $C_2H_6$  or dust Q-curves, probably indicating increased jet activity while data from this grating setting were acquired.

emission in this spectral region that cannot be attributed to CH<sub>3</sub>OH.

[30] Water production rates were derived on four dates (Table 3) based on the detection of ten lines from four hotbands. These values are in reasonable agreement with production rates derived on these dates (and during this time period) using other techniques [Table 3, *Hicks and Fink*, 1997; *Gérard et al.*, 1998; *Bertaux et al.*, 1998; *Combi et al.*, 1998]. Serial observations of OH and O(<sup>1</sup>D) in Hyakutake in March and April 1996 suggest variable comet activity as evidenced by significant fluctuations in derived water production rate from day to day [*Hicks and Fink*, 1997; *Gérard et al.*, 1998]. Indeed, there is evidence of variability on a smaller timescale; regular fluctuations in dust and OH production are seen between UT March 23–25 associated with the 6.23-hour period of the comet [*Schleicher et al.*, 1998; see also *Lisse et al.*, 1999]. Also, there is evidence that the comet experienced a substantial increase in activity on about UT March 22, just prior to our March observations [*Gérard et al.*, 1998; *Schleicher et al.*, 1998; *Lisse et al.*, 1999].

[31] The mixing ratios presented in Table 3 agree within experimental error, suggesting that the chemistry of material released on these three dates was similar. However, we note that C<sub>2</sub>H<sub>6</sub> and H<sub>2</sub>O spectra were obtained closely spaced in time but were not simultaneous, so short-term variability likely affects our derived mixing ratios. The comet rotates almost 30° in 30 min, and so an individual vent could experience a major change in insolation during that time interval, with consequent changes in production. This may be most applicable to mixing ratios derived on UT March 24.5 where there is evidence for variable jet activity within the time of the observations (Figures 4b, 4c, 5, and 6).

[32] Production rates reported in *Mumma et al.* [1996] ( $1.7 \times 10^{29}$  and  $6.4 \times 10^{26}$  s<sup>-1</sup> for water and ethane, respectively, on UT March 24.5) are significantly lower than the values reported in this paper. These differences can be explained as follows. (1) In the present paper, production rates were calculated from extracts 1.5''–11.5'' off the nucleus (in regions not affected by seeing), while in *Mumma et al.* [1996] production rates were determined from a 1'' × 1.4'' extract centered on the nucleus. (2) A simple model was used to determine ethane *g*-factors in *Mumma et al.* [1996], while a more detailed temperature-dependent model was developed to determine *g*-factors in the present work (see *Mumma et al.*, 1996; *Dello Russo et al.*, 2001 for details). We also note that ethane Q-branches assigned as <sup>R</sup>Q<sub>0</sub>, <sup>R</sup>Q<sub>1</sub>, <sup>R</sup>Q<sub>4</sub>, and <sup>R</sup>Q<sub>5</sub> in the study of *Mumma et al.* [1996] should be assigned as <sup>P</sup>Q<sub>1</sub>, <sup>R</sup>Q<sub>0</sub>, <sup>R</sup>Q<sub>3</sub>, and <sup>R</sup>Q<sub>4</sub>, respectively (this changes the derived ethane production rate in the study of *Mumma et al.* [1996] to  $5.0 \times 10^{26}$  s<sup>-1</sup>). (3) *Mumma et al.* [1996] omitted a factor of (2/π) from their expression for production rates (see their endnote 20), making their nucleus-centered production rates systematically too large. (4) The ethane ν<sub>7</sub> band *g*-factor used in the present work is based on the work of *Dang-Nhu et al.* [1984], and is 36% smaller than the band *g*-factor used in the study of *Mumma et al.* [1996]. Water *g*-factors used in the study of *Mumma et al.* are based on a rotational temperature of 70 K, while a 90 K rotational temperature is assumed in the present work. When these factors are accounted for, the apparent disagreement in derived C<sub>2</sub>H<sub>6</sub>

and H<sub>2</sub>O production rates on UT March 24.5 in the present work and that in the study of *Mumma et al.* [1996] are reconciled.

[33] This work revises and extends the initial discovery results of *Mumma et al.* [1996] for UT March 24.5. In addition, this work reports rotational temperatures and production rates on four additional dates. The spatial distribution of H<sub>2</sub>O, C<sub>2</sub>H<sub>6</sub>, and dust are also examined, providing new insights into temporal variability in this comet.

[34] **Acknowledgments.** This work was supported by the NASA Planetary Atmospheres Program under NAG5-7753 and NAG5-10795 to N. Dello Russo, by the NASA Planetary Astronomy Program under RTOP 344-32-30-07 to M. J. Mumma and grant NAG5-7905 to M. A. DiSanti, and by the National Science Foundation under grant AST-9619461 to K. Magee-Sauer. We are thankful for the use of CSHELL, which has been a workhorse for high-resolution infrared studies of comets. We are grateful for the outstanding support from the staff at the NASA Infrared Telescope Facility operated by The University of Hawaii under contract to NASA.

## References

- Bertaux, J. L., J. Costa, E. Quémerais, R. Lallement, M. Berthé, E. Kyrölä, W. Schmidt, T. Summanen, T. Mäkinen, and C. Goukenleuque, Lyman-alpha observations of comet Hyakutake with SWAN on SOHO, *Planet. Space Sci.*, 46, 555–568, 1998.
- Biver, N., et al., Spectroscopic monitoring of comet C/1996 B2 (Hyakutake) with the JCMT and IRAM radio telescopes, *Astron. J.*, 118, 1850–1872, 1999.
- Bockelée-Morvan, D., and J. Crovisier, The nature of the 2.8-μm emission feature in cometary spectra, *Astron. Astrophys.*, 216, 278–283, 1989.
- Bockelée-Morvan, D., P. Colom, J. Crovisier, D. Despois, and G. Paubert, Microwave detection of hydrogen sulphide and methanol in Comet Austin (1989c1), *Nature*, 350, 318–320, 1991.
- Bockelée-Morvan, D., T. Y. Brooke, and J. Crovisier, On the origin of the 3.2- to 3.6-μm emission features in comets, *Icarus*, 116, 18–39, 1995.
- Brooke, T. Y., A. T. Tokunaga, and R. F. Knacke, Detection of the 3.4 micron emission feature in comets P/Brorsen-Metcalf and Okazaki-Levy-Rudenko (1989r) and an observational summary, *Astron. J.*, 101, 268–278, 1991.
- Brooke, T. Y., A. T. Tokunaga, H. A. Weaver, J. Crovisier, D. Bockelée-Morvan, and D. Crisp, Detection of acetylene in the infrared spectrum of comet Hyakutake, *Nature*, 383, 606–608, 1996.
- Chyba, C. F., C. Sagan, and M. J. Mumma, The heliocentric evolution of cometary infrared spectra: Results from an organic grain model, *Icarus*, 79, 362–381, 1989.
- Combes, M., et al., Infrared sounding of comet Halley from Vega 1, *Nature*, 321, 266–268, 1986.
- Combes, M., et al., The 2.5–12 μm spectrum of comet Halley from the IKS-VEGA experiment, *Icarus*, 76, 404–436, 1988.
- Combi, M. R., M. E. Brown, P. D. Feldman, H. U. Keller, R. R. Meier, and W. H. Smyth, Hubble Space Telescope ultraviolet imaging and high-resolution spectroscopy of water photodissociation products in comet Hyakutake (C/1996 B2), *Astrophys. J.*, 494, 816–821, 1998.
- Crovisier, J., K. Leech, D. Bockelée-Morvan, T. Y. Brooke, M. S. Hanner, B. Altieri, H. U. Keller, and E. Lellouch, The spectrum of comet Hale-Bopp (C/1995 O1) observed with the Infrared Space Observatory at 2.9 astronomical units from the sun, *Science*, 275, 1904–1907, 1997.
- Dang-Nhu, M., A. S. Pine, and W. J. Lafferty, Les intensités dans les bandes ν<sub>5</sub>, ν<sub>7</sub>, et ν<sub>8</sub> + ν<sub>11</sub> de l'éthane <sup>12</sup>C<sub>2</sub>H<sub>6</sub>, *Can. J. Phys.*, 62, 512–519, 1984.
- Dello Russo, N., M. A. DiSanti, M. J. Mumma, K. Magee-Sauer, and T. W. Rettig, Carbonyl sulfide in comets C/1996 B2 (Hyakutake) and C/1995 O1 (Hale-Bopp): Evidence for an extended source in Hale-Bopp, *Icarus*, 135, 377–388, 1998.
- Dello Russo, N., M. J. Mumma, M. A. DiSanti, K. Magee-Sauer, R. Novak, and T. W. Rettig, Water production and release in comet C/1995 O1 Hale-Bopp, *Icarus*, 143, 324–337, 2000.
- Dello Russo, N., M. J. Mumma, M. A. DiSanti, K. Magee-Sauer, and R. Novak, Ethane production and release in comet C/1995 O1 Hale-Bopp, *Icarus*, 153, 162–179, 2001.
- DiSanti, M. A., M. J. Mumma, T. R. Geballe, and J. K. Davies, Systematic observations of methanol and other organics in comet P/Swift-Tuttle: Discovery of new spectral structure at 3.42 μm, *Icarus*, 116, 1–17, 1995.
- DiSanti, M. A., M. J. Mumma, N. Dello Russo, K. Magee-Sauer, R. Novak,

- and T. W. Rettig, Half the carbon monoxide of comet Hale-Bopp originates from nuclear ices, *Nature*, 399, 662–665, 1999.
- DiSanti, M. A., M. J. Mumma, N. Dello Russo, K. Magee-Sauer, R. Novak, and T. W. Rettig, Spatially resolved carbon monoxide emission in comet Hale-Bopp: Production rates and rotational temperatures vs. heliocentric distance, *Icarus*, 153, 361–390, 2001.
- Encenaz, T., and R. Knacke, Carbonaceous compounds in comets: Infrared observations, in *Comets in the Post-Halley Era*, edited by R. L. Newburn, M. Nuegebauer, and J. Rahe, pp. 107–138, Kluwer Acad., Norwell, Mass., 1991.
- Gérard, E., J. Crovisier, P. Colom, N. Biver, D. Bockelee-Morvan, and H. Rauer, Observations of the OH radical in comet C/1996 B2 (Hyakutake) with the Nancay radio telescope, *Planet. Space Sci.*, 46, 569–577, 1998.
- Greene, T. P., A. T. Tokunaga, D. W. Toomey, and J. B. Carr, CSHELL: A high spectral resolution 1–5  $\mu\text{m}$  cryogenic echelle spectrograph for the IRTF, *Proc. SPIE Int. Soc. Opt. Eng.*, 1946, 313–324, 1993.
- Hicks, M. D., and U. Fink, Spectrophotometry and the development of emissions for C/1996 B2 (comet Hyakutake), *Icarus*, 127, 307–318, 1997.
- Hoban, S., M. J. Mumma, D. C. Reuter, M. DiSanti, and R. R. Joyce, A tentative identification of methanol as the progenitor of the 3.52- $\mu\text{m}$  emission feature in several comets, *Icarus*, 93, 122–134, 1991.
- Huebner, J., J. Keady, and S. P. Lyon, Solar photo rates for planetary atmospheres and atmospheric pollutants, *Astrophys. Space Sci.*, 195, 1–294, 1992.
- Kunde, V. G., and J. C. Maguire, Direct integration transmittance model, *J. Quant. Spectrosc. Radiat. Transfer*, 14, 803–817, 1974.
- Larson, H. P., H. A. Weaver, M. J. Mumma, and S. Drapatz, Airborne infrared spectroscopy of comet Wilson (19861) and comparisons with comet Halley, *Astrophys. J.*, 338, 1106–1114, 1989.
- Lisse, C. M., Y. R. Fernández, A. Kundu, M. F. A’Hearn, A. Dayal, L. K. Deutsch, G. G. Fazio, J. L. Hora, and W. F. Hoffmann, The nucleus of comet Hyakutake (C/1996 B2), *Icarus*, 140, 189–204, 1999.
- Magee-Sauer, K., M. J. Mumma, M. A. DiSanti, N. Dello Russo, and T. W. Rettig, Infrared spectroscopy of the  $\nu_3$  band of hydrogen cyanide in comet C/1995 O1 Hale-Bopp, *Icarus*, 142, 498–508, 1999.
- Magee-Sauer, K., M. J. Mumma, M. A. DiSanti, and N. Dello Russo, Hydrogen cyanide in comet C/1996 B2 Hyakutake, *J. Geophys. Res.*, 107(0), XXXX, doi:10.1029/2002JE001863, in press, 2002.
- Mumma, M. J., H. A. Weaver, H. P. Larson, D. S. Davis, and M. Williams, Detection of water vapor in Halley’s Comet, *Science*, 232, 1523–1528, 1986.
- Mumma, M. J., M. A. DiSanti, A. Tokunaga, and E. E. Roettger, Ground-based detection of water in comet Shoemaker-Levy 1992 XIX; probing cometary parent molecules by hot-band fluorescence, *Bull. Am. Astron. Soc.*, 27, 1144, 1995a.
- Mumma, M. J., M. A. DiSanti, and X. Xie, *IAUC*, # 6228, 1995b.
- Mumma, M. J., M. A. DiSanti, N. Dello Russo, M. Fomenkova, K. Magee-Sauer, C. Kaminski, and D. X. Xie, Detection of abundant ethane and methane, along with carbon monoxide and water, in comet C/1996 B2 Hyakutake: Evidence for processed interstellar ice, *Science*, 272, 1310–1314, 1996.
- Mumma, M. J., M. A. DiSanti, N. Dello Russo, K. Magee-Sauer, and T. W. Rettig, Detection of depleted ethane in comet 21P/Giacobini-Zinner: Evidence for variable chemistry in the outer solar nebula, *Astrophys. J.*, 531, L155–L160, 2000.
- Mumma, M. J., et al., A survey of organic volatile species in comet C/1999 H1 (Lee) using NIRSPEC at the Keck Observatory, *Astrophys. J.*, 546, 1183–1193, 2001a.
- Mumma, M. J., N. Dello Russo, M. DiSanti, K. Magee-Sauer, R. E. Novak, S. Brittain, T. Rettig, I. S. McLean, D. C. Reuter, and H. Li-Xu, The startling organic composition of C/1999 S4 (Linear): a comet formed near Jupiter?, *Science*, 292, 1334–1339, 2001b.
- Mumma, M. J., N. Dello Russo, M. A. DiSanti, K. Magee-Sauer, R. Novak, A. Conrad, and F. Chaffee, *IAUC*, # 7578, 2001c.
- Reuter, D. C., The contribution of methanol to the 3.4 micron emission feature in comets, *Astrophys. J.*, 386, 330–335, 1992.
- Rothman, L. S., et al., The HITRAN molecular database: Editions of 1991 and 1992, *J. Quant. Spectrosc. Radiat. Transfer*, 48, 469–507, 1992.
- Schleicher, D. G., R. L. Millis, D. J. Osip, and S. M. Lederer, Activity and the rotation period of comet Hyakutake (1996 B2), *Icarus*, 131, 233–244, 1998.
- Weaver, H. A., M. J. Mumma, and H. P. Larson, Infrared investigation of water in comet P/Halley, *Astron. Astrophys.*, 187, 411–418, 1987.
- Weaver, H. A., T. Y. Brooke, G. Chin, S. J. Kim, D. Bockelee-Morvan, and J. K. Davies, Infrared spectroscopy of Comet Hale-Bopp, *Earth Moon Planets*, 78, 71–80, 1999a.
- Weaver, H. A., W. Vacca, N. Biver, S. Kim, D. Bockelee-Morvan, J. Crovisier, T. Brooke, G. Chin, and J. K. Davies, *IAUC*, # 7198, 1999b.
- Weaver, H. A., G. Chin, D. Bockelee-Morvan, J. Crovisier, T. Y. Brooke, D. P. Cruikshank, T. R. Geballe, S. J. Kim, and R. Meier, An infrared investigation of volatiles in Comet 21P/Giacobini-Zinner, *Icarus*, 142, 482–497, 1999c.
- Xie, X., and M. J. Mumma, Monte Carlo simulation of cometary atmospheres: Application to comet P/Halley at the time of the Giotto spacecraft encounter, II, Axisymmetric model, *Astrophys. J.*, 464, 457–475, 1996.

N. Dello Russo and M. A. DiSanti, Department of Physics, Catholic University of America, Washington, DC 20064, USA. (ysndr@lepvax.gsfc.nasa.gov)

K. Magee-Sauer, Department of Chemistry and Physics, Rowan University, Glassboro, NJ 08028, USA.

M. J. Mumma, Laboratory for Extraterrestrial Physics, NASA Goddard Space Flight Center, Code 690.2, Greenbelt, MD 20771, USA.